Yb^{3+} to Er^{3+} energy transfer in $LiNbO_3$

1998 J. Phys.: Condens. Matter 10 8893

(http://iopscience.iop.org/0953-8984/10/39/023)

J. Phys.: Condens. Matter **10** (1998) 8893–8903. Printed in the UK PII: S0953-8984(98)94230-8

Yb^{3+} to Er^{3+} energy transfer in $LiNbO_3$

E Cantelar, J A Muñoz, J A Sanz-García and F Cusso†

Departamento de Física de Materiales, C-IV, Universidad Autónoma de Madrid, 28049 Madrid, Spain

Received 13 May 1998

Abstract. The energy transfer between Yb^{3+} and Er^{3+} ions in lithium niobate is investigated and modelled using the rate equation formalism. An efficient energy transfer from Yb^{3+} to Er^{3+} is found and the transfer and back-transfer coefficients have been determined ($C_{25} = 2.4 \times 10^{-16}$ cm^3 s^{-1} and $C_{52} = 1.8 \times 10^{-16}$ cm^3 s^{-1}, respectively). Using the rate equation formalism it is shown that population inversion of the Er^{3+} $^4I_{13/2}$ level (upper laser level at 1.55 μm) is attainable at sufficiently low pumping levels, making this material suitable for laser applications. The effective transfer efficiency is also calculated, showing good agreement with the experimental values obtained from the increase of the 1.55 μm emission.

1. Introduction

The laser emission of trivalent erbium ions around 1.55 μm, associated with the $^4I_{13/2} \rightarrow {}^4I_{15/2}$ transition, combined with the prospect of using laser diodes as pump sources, has made this ion play a leading role in opto-electronic applications [1, 2].

When used as dopant in lithium niobate ($LiNbO_3$) the combination of the emitting properties of Er^{3+} with the electro-optic, acousto-optic and non-linear properties of the host, together with the possibility of producing low-loss waveguides, it has become an excellent material in order to develop monolithic integrated devices [3, 4].

The principal drawback that presents this ion is its low absorption cross section in the laser diodes emission range (0.8–1.5 μm), which limits the pump efficiency. A possible improvement consists in co-doping the material with a second ion that acts as a sensitizer of the active ion. Ytterbium is the ideal candidate to play this role, not only because of its high absorption cross section but also because of the broad absorption band that offers excitation tuning in the 875–1000 nm wavelength region and the large overlap between ytterbium emission and erbium absorption which allows resonant energy transfer from Yb^{3+} to Er^{3+}.

Yb^{3+}/Er^{3+} co-doped systems are currently being explored and the so-called erbium-ytterbium doped fibre amplifier (EYDFA) or erbium-ytterbium doped waveguide amplifier (EYDWA) have already been demonstrated in co-doped glasses [5–7].

In this work, the energy transfer between Yb^{3+} and Er^{3+} ions in $LiNbO_3$, under Ti-sapphire pumping, is investigated. An efficient energy transfer from Yb^{3+} to Er^{3+} was found and the transfer and back-transfer coefficients have been determined. Using the rate equation formalism it is shown that population inversion is attained at sufficiently

† E-mail address: fernando.cusso@uam.es.

0953-8984/98/398893+11$19.50

low pumping levels, making this an excellent candidate for laser applications. The effective transfer efficiency is also calculated, showing good agreement with the experimental values obtained from the increase of the 1.55 μm emission.

2. Experimental

Single crystals of Er^{3+} and Yb^{3+} co-doped $LiNbO_3$ have been grown by the Czochralski method with automatic diameter control by crucible weighting system [8]. The starting materials were congruent $LiNbO_3$ and erbium and ytterbium oxides. The crystals have a fixed Er^{3+} concentration (0.5 [Er]/[Nb] (%)) and four different Yb^{3+} concentrations (0.1; 0.5; 1.0; 1.5 [Yb]/[Nb] (%) in the melt). Rare-earth concentrations in the crystal, as determined from x-ray fluorescence spectrometry are summarized in table 1.

Table 1. Er^{3+} and Yb^{3+} concentrations in different crystals.

	Melt (%)		Crystal (10^{20} at. cm^{-3})	
Crystal	[Er]/[Nb]	[Yb]/[Nb]	[Er]	[Yb]
1	0.50	0.10	1.13	0.21
2	0.50	0.50	1.27	1.13
3	0.50	1.00	1.02	2.17
4	0.50	1.50	1.19	3.69

Absorption spectra were recorded with a Hitachi spectrophotometer, model U-3501. The emission spectra were obtained under CW excitation with a titanium-sapphire laser pumped with an Ar ion laser or quasi-CW excitation using a MOPO. The fluorescence was analysed through a McPherson monochromator and then detected by InGaAs and/or silicon photodiodes.

3. Results and discussion

3.1. General spectroscopic properties and rate equations

Figure 1 shows the unpolarized absorption spectra of (a) erbium doped and (b) erbium-ytterbium co-doped lithium niobate crystals, in the 1 μm wavelength region. The spectra correspond to excitation beam parallel to the *c*-axis in *z*-cut samples. In the Er-doped crystals the absorption band corresponds to the $^4I_{15/2} \rightarrow {}^4I_{11/2}$ transition of Er^{3+} ions, while in the Er-Yb co-doped crystal the absorption spectrum corresponds to the superposition of this transition plus the $^2F_{7/2} \rightarrow {}^2F_{5/2}$ transition of Yb^{3+} ions (see the energy diagram, figure 2). Both absorption bands overlap in the wavelength range 960–990 nm and the co-doped sample can be excited in a wider range (880–1030 nm) thanks to the higher splitting of the $^2F_{5/2}$ multiple of Yb^{3+} ions.

The existence of energy transfer between the two rare-earth ions can be conveniently visualized by pumping in the 900–950 nm range, where the selective excitation of ytterbium ions, with no overlap with erbium excitation, takes place. After excitation at 917 nm, which corresponds to the shorter wavelength absorption band of Yb^{3+} ions ($^2F_{7/2} \rightarrow {}^2F_{5/2}$), the IR emission spectra of the co-doped samples consists of two emission bands around 1.5 μm and 1.0 μm (figure 3). These bands correspond to the $^4I_{13/2} \rightarrow {}^4I_{15/2}$ erbium transition

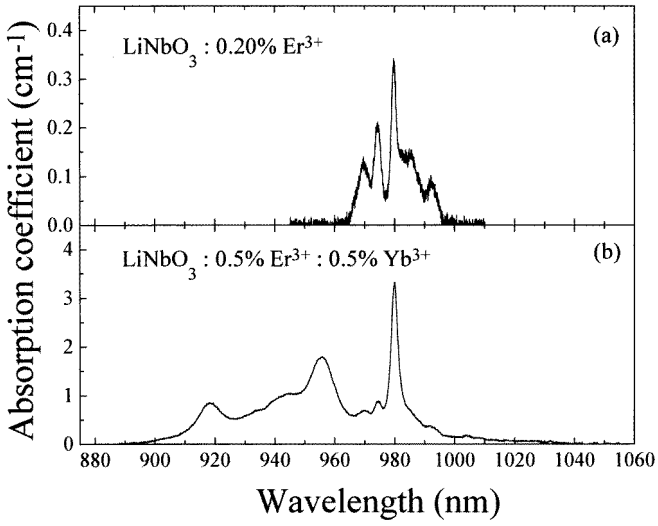

Figure 1. Absorption spectra of (a) Er^{3+} and (b) Er^{3+}/Yb^{3+} doped $LiNbO_3$ in the common excitation range ($^4I_{15/2} \rightarrow {}^4I_{11/2}$ (Er^{3+}) and $^2F_{7/2} \rightarrow {}^2F_{5/2}$ (Yb^{3+}) transitions).

(figure 3(a)) and to the $^4I_{11/2} \rightarrow {}^4I_{15/2}$ and $^2F_{5/2} \rightarrow {}^2F_{7/2}$ erbium and ytterbium emissions, respectively (figure 3(b)).

Further confirmation of the non-radiative character of this transfer is obtained from the decrease observed in the measured lifetime of Yb^{3+} from 580 μs, reported in pure Yb^{3+} doped $LiNbO_3$ [9], to 290 μs measured in the 1 Er^{3+}/Yb^{3+} co-doped crystal (0.1 [Yb]/[Nb] (%)), indicating that a new de-excitation channel of the $^2F_{5/2}Yb^{3+}$ multiplet is activated.

Figure 2 presents a schematic illustration of the energy levels of Yb^{3+} and Er^{3+} ions, and the relevant transitions involved after Yb^{3+} excitation, including energy transfer and cooperative up-conversion processes, according to the standard description of Er^{3+}/Yb^{3+} co-doped materials, proposed by Johnson *et al* [10] in the early seventies, and customarily used to describe the Yb^{3+} to Er^{3+} energy transfer processes [11, 12].

After excitation of the Yb^{3+} ions they may relax (mostly radiatively) to the ground state or transfer to the $^4I_{11/2}$ level of Er^{3+} ions, from where it may relax within the same ions or be transferred back to Yb^{3+}.

In the de-excitation of the $^4I_{11/2}$ level of Er^{3+}, it gives luminescence in the 1.0 μm range associated with the $^4I_{11/2} \rightarrow {}^4I_{15/2}$ transition (figure 3(b)) or in the 1.5 μm range corresponding to the $^4I_{13/2} \rightarrow {}^4I_{15/2}$ transition (figure 3(a)). The $^4I_{13/2}$ level is populated mostly through a non-radiative channel from the upper $^4I_{11/2}$ level [13, 14].

Additionally, a cooperative up-conversion process can also take place via the transfer of a second photon from the Yb^{3+} to Er^{3+}, according to the mechanism ($^2F_{5/2} \rightarrow {}^2F_{7/2}$ (Yb^{3+}): $^4I_{11/2} \rightarrow {}^4F_{7/2}$ (Er^{3+})). In accordance with the spectroscopic properties of Er^{3+} in lithium niobate [13, 14], the $^4F_{7/2}$ multiplet relaxes non-radiatively to the $^4S_{3/2}$ level, from where the relaxation is partially radiative to the ground state (green emission at around 550 nm) and partially non-radiative to the $^4I_{11/2}$. The intermediate levels ($^4F_{9/2}$ and $^4I_{9/2}$) experience a fast non-radiative decay so that their populations (and contributions to luminescence) can be ignored.

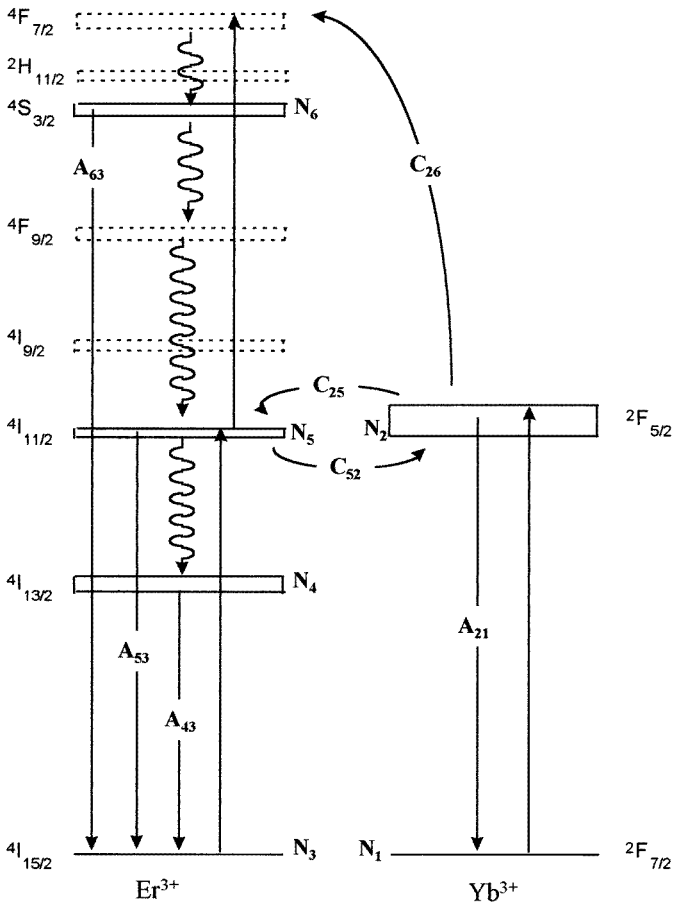

Figure 2. Schematic energy level diagram of $LiNbO_3:Er^{3+}/Yb^{3+}$ showing the multiplets involved in the energy transfer, up-conversion processes and principal emissions.

According to this model, the Yb^{3+}/Er^{3+} transfer dynamics is described, in general, by the following rate equations [10–12]

$$\frac{dN_2}{dt} = \sigma_{Yb}\phi N_1 - (A_{21} + W_{21}^{NR})N_2 - C_{25}N_2N_3 + C_{52}N_5N_1 - C_{26}N_2N_5 \quad (1)$$

$$\frac{dN_4}{dt} = (A_{54} + W_{54}^{NR})N_5 + A_{64}N_6 - (A_{43} + W_{43}^{NR})N_4 \quad (2)$$

$$\frac{dN_5}{dt} = (A_{65} + W_{65}^{NR})N_6 + C_{25}N_2N_3 - C_{52}N_5N_1 - C_{26}N_2N_5 - (A_{54} + A_{53} + W_{54}^{NR})N_5 \quad (3)$$

$$\frac{dN_6}{dt} = C_{26}N_2N_5 - (A_{65} + A_{64} + A_{63} + W_{65}^{NR})N_6 \quad (4)$$

$$N_3 + N_4 + N_5 + N_6 = N_{Er} \quad (5)$$

$$N_1 + N_2 = N_{Yb} \quad (6)$$

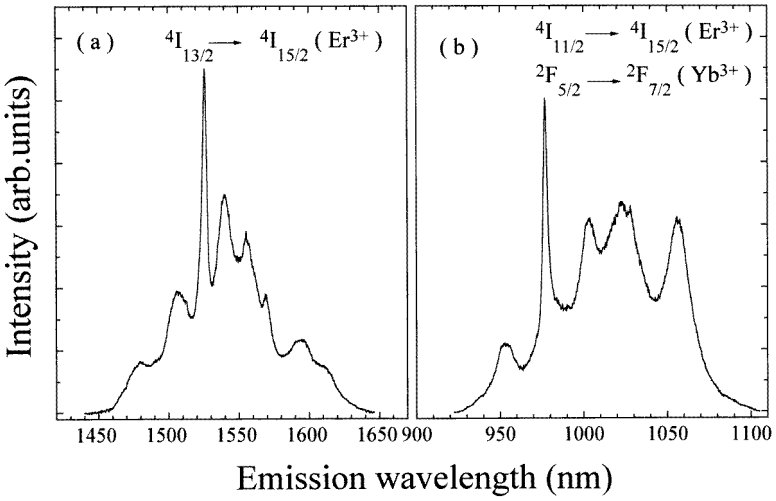

Figure 3. IR emission spectra of $LiNbO_3:Er^{3+}/Yb^{3+}$. (a) $^4I_{13/2} \rightarrow {}^4I_{15/2}$ (Er^{3+}) transition and (b) overlap between $^4I_{11/2} \rightarrow {}^4I_{15/2}$ (Er^{3+}) and $^2F_{5/2} \rightarrow {}^2F_{7/2}$ Er^{3+} and (Yb^{3+}) emissions.

where N_i is the population of the i-level (in units of cm^{-3}), A_{ij} and W_{ij}^{NR} the radiative and non-radiative transition probabilities between the I and j states (in units of s^{-1}), σ_{Yb} (in units of cm^2) is the Yb^{3+} absorption cross section at the pumping wavelength, ϕ is the pumping flux (in units of cm^{-2} s^{-1}), and finally C_{25}, C_{52} and C_{26} are coefficients (in units of cm^3 s^{-1}) which quantify the energy transfer, the back-transfer and the up-conversion processes, respectively.

The term $C_{25}N_2N_3$, which quantifies the transfer rate (in units of cm^{-3} s^{-1}) describes a cross relaxation process between two ions (Yb^{3+} and Er^{3+}); the first ion (Yb^{3+}) in the $^2F_{5/2}$ excited state (with population N_2) and the second (Er^{3+}) in the $^4I_{15/2}$ ground state (with population N_3) which ends with the Yb^{3+} ion in the $^2F_{7/2}$ ground state and the Er^{3+} ion in the $^4I_{11/2}$ excited state. The opposite process occurs in the back transfer ($C_{52}N_5N_1$).

Finally, the term $C_{26}N_2N_5$ quantifies the cross relaxation up-conversion process leading to the excitation of the $^4F_{7/2}$ Er^{3+} level, according to the mechanism ($^2F_{5/2} \rightarrow {}^2F_{7/2}$ (Yb^{3+}): $^4I_{11/2} \rightarrow {}^4F_{7/2}$ (Er^{3+})).

3.2. CW pumping and energy transfer rates

The transfer and back transfer coefficients, C_{25} and C_{52}, can be experimentally obtained through the comparison of the emission intensities at 1.0 μm and 1.5 μm under continuous excitation with low-pumping flux.

When the steady state is reached, under continuous illumination, all the derivatives in equations (1)–(6) become equal to zero. Also, in the weak pumping limit which is used for spectroscopic characterization, it is possible to assume that $N_1 \approx N_{Yb}$, $N_3 \approx N_{Er}$ and it is also possible to neglect the up-conversion terms ($N_2N_5 \approx 0 \Rightarrow N_6 \approx 0$). The equations (1)–(6) lead to

$$N_1 \approx N_{Yb} \tag{7}$$

$$N_2 = \frac{\sigma_{Yb}\phi N_1}{A_{2m} + C_{25}N_3(A_{5m}/(C_{52}N_1 + A_{5m})} \tag{8}$$

$$N_3 \approx N_{Er} \tag{9}$$

$$N_4 = \frac{A_{5m} - A_{53}}{A_{43}} N_5 \tag{10}$$

$$N_5 = \frac{C_{25} N_2 N_3}{C_{52} N_1 + A_{5m}} \tag{11}$$

where $A_{2m} = A_{21} + W_{21}^{NR} = \tau_{2,exp}^{-1}$ and $A_{5m} = A_{54} + A_{53} + W_{54}^{NR} = \tau_{5,exp}^{-1}$ represent the total de-excitation probabilities, which can be obtained from the reciprocal of the measured lifetimes ($\tau_{2,exp}$ and $\tau_{5,exp}$) of levels $^2F_{5/2}$ and $^4I_{11/2}$, respectively.

The simplified energy level scheme is now given in figure 4(a) together with the transitions relevant to the method used to calculate the Yb^{3+}/Er^{3+} transfer coefficients.

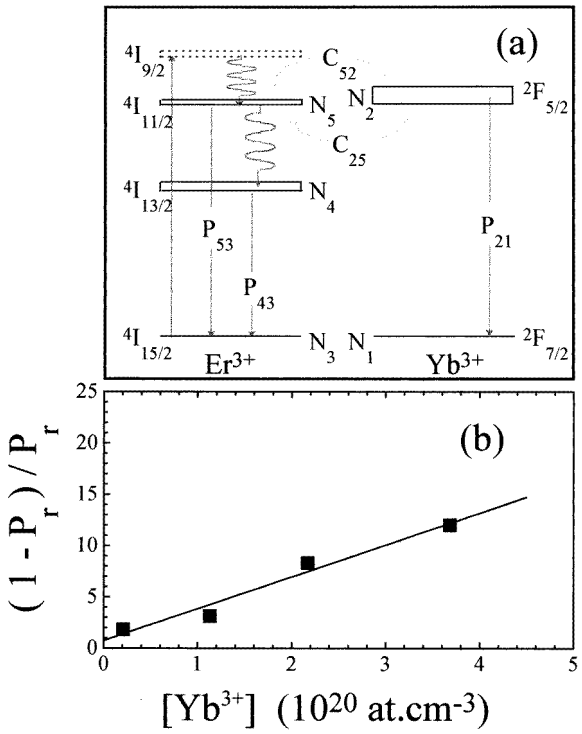

Figure 4. (a) Energy level scheme and transitions used to evaluate the transfer and back-transfer rates. (b) Relationship between the ratio (P_r) of the Er^{3+} emission around 1 μm over the total Er^{3+}/Yb^{3+} at the same wavelength as a function of Yb^{3+} concentration. From the linear fitting using equation (13) the transfer and back transfer rates (C_{25} and C_{52}) are calculated.

The erbium ions are excited to the $^4I_{9/2}$ multiplet using a Ti-sapphire laser at 800 nm ($^4I_{15/2} \rightarrow {}^4I_{9/2}$). From the $^4I_{9/2}$ level, the Er^{3+} ion relaxes non-radiatively to the $^4I_{11/2}$ multiplet. Then, either radiative and non-radiative intra-erbium relaxation or energy transfer to ytterbium ions can occur (see figure 4(a)), so that the comparison between the emission intensities at 1.0 μm ($^4I_{11/2} \rightarrow {}^4I_{15/2}$ and $^2F_{5/2} \rightarrow {}^2F_{7/2}Er^{3+}$ and Yb^{3+}, respectively) and 1.5 μm ($^4I_{13/2} \rightarrow {}^4I_{15/2}$ Er^{3+}) for different Er^{3+}/Yb^{3+} concentrations allows the determination of the transfer coefficients [10–12].

In fact, the ratio (P_r) of the Er^{3+} emission around 1 μm (P_{53}) over the total Er^{3+}/Yb^{3+} emission ($P_{53} + P_{21}$) also around 1 μm ($\nu_{53} \approx \nu_{21}$) can be expressed as

$$P_r = \frac{P_{53}}{P_{53} + P_{21}} = \frac{A_{53}C_{25}N_{Er}}{A_{53}C_{25}N_{Er} + A_{21}(C_{52}N_{Yb} + A_{5m})} \tag{12}$$

where $P_{ij} \propto \int I_{ij}(\lambda)\,\mathrm{d}\lambda$, being $I_{ij}(\lambda)$ the measured emission intensity for the $i \rightarrow j$ transition.

Equation (12) can be conveniently rearanged as

$$\frac{1 - P_r}{P_r} = \left(\frac{A_{21}A_{5m}}{A_{53}C_{25}N_{Er}}\right) + \left(\frac{A_{21}C_{52}}{A_{53}C_{25}N_{Er}}\right) N_{Yb} \equiv \alpha + \beta N_{Yb}. \tag{13}$$

So measuring the ratio P_r for samples with fixed Er^{3+} concentration and variable ytterbium concentrations, a representation of the quantity $(1 - P_r)/P_r$ as a function of the ytterbium concentration, should give a linear dependence with slope β and intercept α, from where the transfer and back-transfer coefficients are calculated

$$C_{52} = \frac{\beta}{\alpha} A_{5m} \tag{14}$$

$$C_{25} = \frac{1}{\alpha} \frac{A_{21}A_{5m}}{A_{53}N_{Er}}. \tag{15}$$

In practice, in co-doped samples it is difficult to measure the erbium emission around 1 μm (P_{53}) independently of the Yb^{3+} emission, due to the strong overlap between $^4I_{11/2} \rightarrow {}^4I_{15/2}$ (Er^{3+}) and $^2F_{5/2} \rightarrow {}^2F_{7/2}$ (Yb^{3+}) emissions (see figure 3(b)), so that the standard procedure [10–12] is to compare the overall Yb^{3+}/Er^{3+} emission at 1 μm ($P_{53} + P_{21}$) with 1.5 μm emission of the Er^{3+} ions (P_{43}), which ratio with the Er^{3+} 1 μm emission can be evaluated from samples singly doped with Er^{3+}

$$P_r = \frac{P_{43}}{P_{53} + P_{21}} \left(\frac{P'_{53}}{P'_{43}}\right) \tag{16}$$

where P'_{53}/P'_{43} represents the emission intensities ratio in an erbium doped sample. Then all the quantities in the last expression can be obtained from direct experimental measurements.

In this work, the emissions at 1.5 μm and 1 μm have been measured for the set of four crystals co-doped with fixed Er^{3+} concentration and different Yb^{3+} concentrations (table 1). The ratio $(1 - P_r)/P_r$, calculated from those measurements is represented in figure 4(b) as a function of the Yb^{3+} concentration. It can be observed that, according to equation (13), a linear dependence is observed. From the least squares fitting of this data, and using the values reported in the literature [9, 13] for the Er^{3+} and Yb^{3+} transition probabilities (which have been summarized in table 2) the transfer coefficients are readily calculated from expressions (14) and (15). The values obtained are $C_{25} = 2.4 \times 10^{-16}$ cm^3 s^{-1} and $C_{52} = 1.8 \times 10^{-16}$ cm^3 s^{-1} for transfer and back-transfer, respectively. Therefore, the transfer coefficient is 1.3 times higher than the back transfer, which is sufficient to provide population inversion via energy transfer as will be shown in the next section.

3.3. Rate equations formalism and population inversion

A first consistency test of the analysis procedure has been the verification that, in the weak pumping limit, the up-conversion terms are negligible, as supposed initially in order to obtain the simplified equations (7)–(11).

Using now the first set of differential equations (1)–(6), where no previous simplification has been adopted, and using the calculated transfer coefficients the population of the different

Table 2. Radiative (A_{ij}) and total ($A_{im} = \tau_{i,exp}^{-1} = \sum_j A_{ij} + W_{ij}^{NR}$) transition probabilities.

Transition	A_{ij}	Probability (10^3 s^{-1})	Reference
$^2F_{5/2} \rightarrow {}^2F_{7/2}$	A_{21}	1.72	9
	A_{2m}	1.72	9
$^4S_{3/2} \rightarrow {}^4I_{11/2}$	A_{65}	0.08	13
$^4S_{3/2} \rightarrow {}^4I_{13/2}$	A_{64}	0.96	13
$^4S_{3/2} \rightarrow {}^4I_{15/2}$	A_{63}	2.73	13
	A_{6m}	40	13
$^4I_{11/2} \rightarrow {}^4I_{13/2}$	A_{54}	0.04	13
$^4I_{11/2} \rightarrow {}^4I_{15/2}$	A_{53}	0.36	13
	A_{5m}	4.55	13
$^4I_{13/2} \rightarrow {}^4I_{15/2}$	A_{43}	0.37	13
	A_{4m}	0.37	13

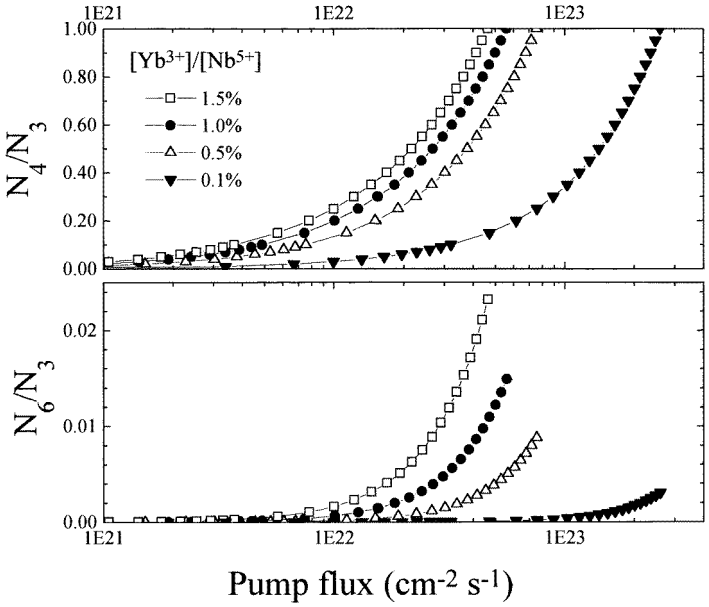

Figure 5. Ratio between the populations of $^4I_{13/2}$ (N_4) and $^4S_{3/2}$ (N_6) to $^4I_{15/2}$ (N_3) Er^{3+} levels, by selective Yb^{3+} excitation at 917 nm, for different pumping rates.

levels involved in the energy transfer processes (see figure 2) can be obtained under steady state conditions for different pumping rates. In so doing, it has been assumed that the up-conversion coefficient is twice the forward transfer one ($C_{26} = 2 \cdot C_{25}$), which is the ratio between the electric dipole strengths of the $^4I_{11/2} \rightarrow {}^4F_{7/2}$ and $^4I_{15/2} \rightarrow {}^4I_{11/2}$ transitions [11, 13].

The results are presented in figure 5, where the Er^{3+} populations (relative to that of the ground state, N_3) are calculated as a function of the pump flux, for the different Yb^{3+} concentrations used in the present work. The lower part of the figure shows the population of the $^4S_{3/2}$ level (N_6), which corresponds to the up-converted population and which is the origin of the Er^{3+} emission at 550 nm. The upper part corresponds to N_4, the population of the $I_{13/2}$ multiplet (upper laser level at 1.5 μm).

It can be observed that the $^4S_{3/2}$ population remains negligibly small for pump fluxes below 10^{22} photons cm^{-2} s^{-1}, which is well above the pumping levels used for spectroscopic characterization. This result confirms that the up-conversion processes can be ignored for our experimental conditions and supports the assumptions leading to the simplified expressions (7)–(11).

The upper part of figure 5 shows that it is possible to generate population inversion of the $^4I_{13/2}$ Er^{3+} multiplet by Yb^{3+} excitation with relatively low-pumping levels, and how this threshold is reduced as the Yb^{3+} concentration increases. The pump needed to reach population inversion is well within the values normally used in standard laser cavities, and below those attainable in structures with high-optical confinement such as channel or planar waveguides [15–17], including those reported in the $LiNbO_3$:Yb^{3+} waveguide lasers [18].

3.4. Effective energy transfer efficiency

Another way of quantifying the effectiveness of Yb^{3+}/Er^{3+} transfer is through the evaluation of the increase in the 1.5 μm emission of erbium ions (per absorbed photon), due to the presence of ytterbium ions [9, 16].

In this case, and at variance with the procedure followed before, the excitation is performed at wavelengths that simultaneously excite both Er^{3+} and Yb^{3+} ions, that is within the range 960 nm $< \lambda_{exc} <$ 990 nm (see figure 1).

From the experimental point of view, the efficiency (η) can be obtained comparing the fluorescence intensities (per absorbed photon, $N_{abs.ph}$) measured at 1.5 μm in a co-doped, I(Er/Yb), and in a singly doped sample, I(Er). The ratio between absorption coefficients at the pump wavelength in the co-doped and in the singly doped samples is obtained from the samples absorption

$$\eta = \frac{I(\mathrm{Er/Yb})/N_{abs.ph}(\mathrm{Er/Yb})}{I(\mathrm{Er})/N_{abs.ph}(\mathrm{Er})}. \tag{17}$$

Alternatively, and in the case of samples always co-doped with fixed Er^{3+} concentration and variable Yb^{3+} concentrations, as is the case in the present work, the comparison of the intensities would give the relative transfer efficiency of the different samples.

Following this procedure, ad 1.5 μm emission of the different samples, with fixed (0.5%) Er^{3+} and variable (0.1–1.5%) Yb^{3+} concentrations, has been measured after 974 nm excitation. These excitations have been chosen because they correspond to common excitation of Er^{3+} and Yb^{3+} ions (see figure 1) while simultaneously the absorption cross sections are sufficiently low to guarantee that the samples are 'optically thin', with a low attenuation of the excitation beam, which preserves the geometry for luminescence collection.

In comparison to the crystal with the lower Yb^{3+} concentrations (0.1%), the luminescence from the other samples is increased 1.15, 1.82 and 2.32 times while the absorption is also increased 1.38, 2.65 and 3.59 times. The relative efficiency, therefore, is reduced to 0.83, 0.69 and 0.65, respectively, for samples with 0.5%, 1.0% and 1.5% Yb^{3+}, respectively.

Using the rate equation formalism it is possible to relate the transfer efficiency with the spectroscopic parameters of the rare-earth ions (Er^{3+} and Yb^{3+}) and the transfer coefficients (C_{25} and C_{52}) previously determined. The only modification needed in the standard rate equations (equations (1)–(6)) is to consider an additional term ($\sigma_{Er}\phi N_3$) in equation (3) to take into account the population of the $^4I_{11/2}$ level by direct excitation of the Er^{3+} ions. In stationary conditions ($\mathrm{d}N_i/\mathrm{d}t = 0$) and for optically thin samples ($N_{abs.ph} \propto \sigma N$), it is

readily obtained

$$\eta = \frac{(A_{5m}/(A_{5m} + C_{52}N_{Yb}))}{(\sigma_{Yb}N_{Yb} + \sigma_{Er}N_{Er})}\left[\frac{C_{25}N_{Er}\sigma_{Yb}N_{Yb}}{C_{25}N_{Er}(A_{5m}/(A_{5m} + C_{52}N_{Yb})) + A_{2m}} + \sigma_{Er}N_{Er}\right] \qquad (18)$$

which allows the calculation of the transfer efficiency from the basic spectroscopic parameters and for arbitrary concentrations of the dopants, N_{Yb}, N_{Er}. It should be reminded that the rare-earth absorption cross sections should correspond to the excitation wavelength used in each case.

The absolute values calculated from equation (18) and using the spectroscopic parameters and transfer coefficients calculated in the previous section are plotted in figure 6 (open circles) together with the experimental values (full circles), where the relative efficiencies have been scaled to that calculated for 0.1% Yb^{3+} concentration ($\eta \approx 60\%$). It can be observed that the relative efficiencies decrease in good accordance with the predictions from equation (18). As it is expected, the efficiency is very high for low Yb^{3+} concentrations, becoming $\eta \approx 100\%$ for negligible Yb^{3+} contents, which reflects the obvious situation that 100% of the photons are emitted by Er^{3+} ions when these are the only absorbent ions. When Yb^{3+} concentration increases these ions absorb more and more photons and a lower fraction reaches the Er^{3+} ions and the emission at 1.5 μm decreases. For the Er^{3+} concentration used in the present work (0.5%) the efficiency decreases abruptly to a value between $\eta \approx 50$–40% at Yb^{3+} concentrations around 0.2%, and then it remains nearly constant in a wide range of Yb^{3+} concentrations.

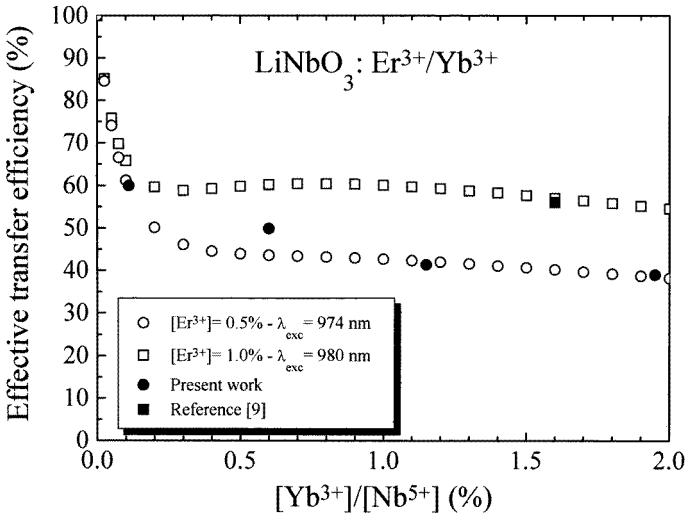

Figure 6. Calculated (open symbols) and experimental (full symbols) effective energy transfer efficiency for $LiNbO_3$:Er^{3+} sensitized with different Yb^{3+} concentrations.

In the same figure is also shown the efficiencies calculated for samples with a higher (1.0%) Er^{3+} concentration (open squares) and a different excitation wavelength ($\lambda_{exc} = 980$ nm), which corresponds to the experimental conditions used by Huang and McCaughan [9] for a $LiNbO_3$ crystal co-doped with 1% Er^{3+}/1.6% Yb^{3+}, where a transfer efficiency $\eta = 61\%$ (full square) is reported. Again it can be seen in good agreement with the predictions from the rate equations calculations. In a similar way to the results for lower concentrations, the efficiency decreases abruptly from $\eta = 100\%$ at 0% Yb concentration

to lower value ($\eta \approx 60\%$, in this case) at around 0.2% Yb concentration, remaining then almost constant for increasing Yb^{3+} concentrations.

4. Conclusion

The Yb^{3+}/Er^{3+} transfer and back-transfer rates have been experimentally determined through comparison of the IR emissions (1 μm and 1.5 μm) of a set of co-doped $LiNbO_3$ samples, with fixed Er^{3+} and variable Yb^{3+} concentrations after excitation to the $^4I_{9/2}$ Er^{3+} multiplet at 800 nm. The results indicate that the Yb^{3+} to Er^{3+} transfer rate is higher than the back-transfer rate (by about a factor 1.3).

Using the rate equation formalism it is found that population inversion would be obtained in $LiNbO_3$:Er^{3+}/Yb^{3+} by Yb^{3+} excitation and energy transfer to Er^{3+} with sufficiently low pumping rates for practical applications.

The effective transfer efficiency, calculated from the transfer rate parameters previously obtained is in good agreement with the experimental determinations from the increase in the 1.55 μm emission in co-doped samples.

These results indicate that Yb^{3+} co-doping provides a suitable way for pumping Er^{3+} ions in lithium niobate, which enhances the prospects for using efficient diode pumping in the 980 nm range for Er^{3+} doped lithium niobate amplifiers and integrated devices.

Acknowledgment

This work was partially supported by CICYT under contract TIC95-0166.

References

[1] Hanna D C and Tropper A C 1991 *Optical Fibre Lasers and Amplifiers* ed P W France (Glasgow and London: Blakie)
[2] Digonnet J F 1993 *Rare Earth Doped Fiber Lasers and Amplifiers* (New York: Dekker)
[3] Brinkman R, Sohler W and Suche H 1991 *Electron. Lett.* **27** 415
[4] Schäfer K, Baumann I, Sohler W, Suche H and Westenhöfer S 1997 *IEEE J. Quantum Electron.* **33** 1636
[5] Tamura K, Yoshida E, Yamada E and Nakazawa M 1996 *Electron. Lett.* **32** 835
[6] Tacheo S, Laporta P, Longhi S, Svelto O and Svelto C 1996 *Appl. Phys.* B **63** 425
[7] Barbier D, Rattay M, Saint André F, Clauss G, Trouillon M, Kevorkian A, Delavaux J M P and Murphy E 1997 *IEEE Phot. Tech. Lett.* **9** 315
[8] Santos M T, Rojo J C, Arizmendi L and Diéguez E 1994 *J. Crystal Growth* **142** 103
[9] Huang C and McCaughan L 1997 *IEEE Phot. Tech. Lett.* **9** 599
[10] Johnson L F, Guggenheim H J, Rich T C and Ostermayer F W 1972 *J. Appl. Phys.* **43** 1152
[11] Zandi B, Merkle L D, Hutchinson J A, Verdun H R and Chai B H T 1994 *J. Physique* IV **C4** 587
[12] Simondi-Teissiere B, Viana B, Vivien D and Lejus A M 1996 *Opt. Mat.* **6** 267
[13] Núñez L, Lifante G and Cussó F 1996 *Appl. Phys.* B **62** 485
[14] Amin J, Dussardier B, Schweizer T and Hempstead M 1996 *J. Lumin.* **69** 17
[15] Vossler G L, Brooks C J and Winik K A 1995 *Electron. Lett.* **31** 1162
[16] Román J E, Camy P, Hempstead M, Brocklesby W S, Nouh S, Béguin A, Lerminaux C and Wilkinson J S 1995 *Electron. Lett.* **31** 1345
[17] Shepherd D P *et al* 1994 *J. Appl. Phys.* **76** 7651
[18] Jones J K, de Sandro J P, Hempstead M, Shepherd D P, Large A C, Tropper A C and Wilkinson J S 1995 *Opt. Lett.* **20** 1477